

Improved two-dimensional product imaging: The real-time ion-counting method

Bor-Yu Chang, Rama C. Hoetzlein, Julie A. Mueller, Joseph D. Geiser, and Paul L. Houston^{a)}

Department of Chemistry, Cornell University, Ithaca, New York 14853-1301

(Received 18 November 1997; accepted for publication 20 January 1998)

A novel ion-counting method for significantly improving the spatial resolution and detection sensitivity of two-dimensional product imaging in molecular beam experiments is presented. The method makes use of real-time digital image processing to retrieve, threshold, and determine the local maximum of each ion hitting a microchannel plate assembly. The current version can process data at rates up to 3.07 Mbyte/s, and methods for accelerating this rate are proposed. © 1998 American Institute of Physics. [S0034-6748(98)03904-5]

I. INTRODUCTION

Two-dimensional product imaging has become an important and sensitive tool in the study of molecular reaction dynamics in recent years.¹⁻⁴ The technique, which allows one to obtain simultaneously the kinetic energy and angular distributions of a state-selected product from a chemical reaction, provides important details about a reaction mechanism. Many state-selective detection schemes have been employed in two-dimensional (2D) product imaging, such as resonance-enhanced multiphoton ionization (REMPI), photoelectron spectroscopy, and laser-induced fluorescence.²⁻⁴

In the original 2D product imaging experiment by Chandler and Houston,¹ products from a unimolecular dissociation were ionized via REMPI, extracted through a time-of-flight mass spectrometer (TOF-MS), and finally recorded by a position sensitive microchannel plate (MCP) detector equipped with a fast-response phosphor screen. A charge-coupled device (CCD) camera and a frame grabber were used to download the images from the phosphor screen to a computer. A product image is a 2D projection of the state-selected photofragment's three-dimensional (3D) recoil velocity distribution. The 3D distribution can be reconstructed by applying the inverse Abel transformation to the 2D product image.^{2,5} The 3D velocity and angular distributions of chemical products provide details of the dynamics and mechanism of a chemical scattering process, such as a bimolecular collision or unimolecular dissociation.⁶

Despite the success of 2D product ion imaging in many fields of physical chemistry, the potential of the technique has not been completely exploited.^{2,3} Several factors affecting the performance of the ion imaging technique are addressed by our real-time ion counting method. First, if the yield of product ions is too low, background noise can surpass the desired ion signal and prevent the camera from acquiring a useful image. In our detector, an important source of this background noise comes from the thermal electrons in the image intensifier of the CCD camera.⁷ In an intensified CCD camera operating at room temperature, a pixel can be-

come saturated by such thermal electrons within about one second. This problem can be overcome by using a cooled CCD camera, but these are usually more expensive and have a lower imaging rate. A second factor is the detector resolution. Although the size of an actual ion ($\sim 10^{-9}$ m) is much smaller than a single resolution element of our detector, the detection of a single ion for an MCP potential of 1700 V across the two-plate assembly typically results in a spot with a radius of 0.2 mm, covering about 5×5 pixels of the CCD camera. This loss of resolution is due primarily to the image intensifier.

When a traditional Wiley-McLaren TOF-MS is used for 2D imaging, the finite volume in which product ions are created leads to further blurring of ions formed with the same velocity vector. The recently developed technique of velocity mapping is used to avoid this blurring.^{8,9} The method employs electrostatic lenses such that all ions with the same initial velocity are focused to the same point on the detector. Thus, the experimental resolution becomes limited by the detector. The new real-time ion-counting method reported here further improves this resolution. The notion of photon counting has been widely applied in optical spectroscopy to recover low-level photon signals from a noisy background. Similarly, our ion counting method discriminates the desired ion signal from the background by using a threshold level to reduce noise. Furthermore, of the group of pixels illuminated by a single ion, only the local maximum of the group is counted as signal. Hence ion counting improves the spatial resolution by locating a single position of ion impact rather than accumulating the entire area of illuminated pixels. This single position corresponds to one counted ion. Therefore, variation in the signal level due to detector inhomogeneity is significantly reduced as well by the ion-counting technique.

Traditional real-time digital image processing is limited by the small number of arithmetic operations that can be performed on an image during the time between data cycles.^{10,11} In 2D ion-counting product imaging, the data rate of imaging is at least ~ 3 Mbyte/s (10 Hz, 640×480 pixels per image) and depends on the repetition rate of the lasers and on the size and data depth of the image. To achieve

^{a)}Electronic mail: plh2@cornell.edu

real-time ion counting at this data rate, new algorithms have been developed to reduce the amount of data and the number of operations required to process an image. These will be addressed in the following sections.

II. EXPERIMENT

The basic scheme of our experiment has been reported elsewhere.¹²⁻¹⁶ Here we briefly describe the system and its revisions. The molecular beam system is similar to that described in Ref. 16, except that a piezoelectric nozzle¹⁷ with an orifice of 500 μm was used in place of the Precision Instruments nozzle. $\text{N}_2(v''=0, J''\approx 74)$ products¹⁸ from the photodissociation of N_2O (15% N_2O in He) were ionized at approximately 203.2 nm using the $a''^1\Sigma_g^+ \leftarrow X^1\Sigma_g^+$ transition first reported by Lykke and Kay¹⁹ and applied to N_2O photodissociation by Hanisco and Kummel.²⁰ A single laser was used both to dissociate the N_2O and to probe a single rotational level of the N_2 . The power of the 203.2 nm light was kept to approximately 200 μJ in order to avoid spatial congestion in the ion images.

An ultraviolet-enhanced, intensified CCD camera (Xy-bion Electronics, ISG-250U) with a macro camera lens (focal length=90 mm, $f/2.8$) is used to collect images. The UV enhancement here is advantageous because the emission spectrum of the phosphor screen (Galileo, P-47) peaks around 400 nm, the wavelength where the spectral response of most CCDs cuts off. The P-47 phosphor was chosen so as to provide good time resolution (80 ns) needed for high mass resolution in the time-of-flight, but it emits in a wavelength region where the camera sensitivity is low. An intensifier is therefore required. The output of the CCD camera is standard EIA RS170 analog interlaced video signal (~ 533 horizontal \times 420 vertical pixels) operating at 30 Hz. Resolution is limited predominantly by the image intensifier of the CCD camera. Since our experiments are performed at 10 Hz, a home-made circuit reduces the 60 Hz vertical drive signal of the camera to a 10 Hz trigger signal which triggers the lasers, the pulsed molecular beam valve, the gate of the CCD image intensifier, and the frame grabber. The gate sent to the CCD image intensifier, about 300 ns in duration, is used to select the mass of the imaged ions. An externally triggered ISA-bus frame grabber (Dipix Technologies, XPG-1000) with 16 MByte of memory and a 50 MHz digital signal processor (DSP) then grabs the image and transfers it to a PC (Gateway 2000) with a Pentium 200 processor. A second monitor with an additional video display card (Dipix Technologies, EDB-200) is used to display acquired images during the experiment.

A typical 8-bit image of 640×480 pixels requires 307 Kbytes of memory. Our experiments are performed at 10 Hz, leading to a data rate of 3.07 Mbyte/s. This rate limits the DSP to an average of 16 operations per pixel per image. More than 20 DSP operations are required to locate the ion centers on the image. Therefore, it is apparently not feasible to perform real-time ion counting using the DSP. One could consider transferring the data directly to the processor and performing the ion counting there. Although the host computer is equipped with a fast processor (Pentium 200), the

ISA bus communicates data from the frame grabber to the PC at 2 Mbyte/s, making it impossible to transfer all images from the frame grabber to the host computer in real time. Thus, it is also apparently not feasible to perform the ion counting using the Pentium processor of the host computer. The new real-time counting algorithm described below overcomes these problems by concentrating only on those pixels which ions have illuminated, thus reducing the data rate.

III. REAL-TIME ION COUNTING

Traditionally, software for the 2D product imaging of ions has been based on the direct accumulation of captured image data. Each source image from the camera is added into a final image buffer.¹²⁻¹⁶ The main problem with this method, as applied to ion imaging, is that the signal from a single ion can cover several pixels in a source image. The intensity distribution approximately follows a two-dimensional Gaussian profile, with the center-of-mass of the charge distribution for a single ion located at the peak. Since many source images are accumulated over time, the effect of the pixel intensity distribution from each ion is analogous to applying a blurring filter over the entire image. Ion counting solves this problem by performing a search over each input image for all local maxima. The result is a set of single pixel addresses corresponding to the center of each peak, so that only one pixel (the local maximum) is counted for each ion incident on the detector. These pixels are then accumulated into a final image buffer.

As discussed in Sec. I, because the input data rate (307 Kbyte for each image at 10 Hz) restricts the processing time, ion counting is performed in only two operational steps for each incoming image. In the first step, a threshold is applied to the original image, such that any pixel intensity lower than the chosen discrimination level will be rejected as noise. Pixel intensity due to an ion is usually much higher than surrounding background noise, so this step effectively removes all low-level noise from the image. In addition, thresholding reduces the data size from 307 K (640×480) per image to an average of 4 K (depending on the number of ions). This reduction provides a smaller data set for the second step and thereby reduces the average number of operations per pixel.

For ion counting, comparison of source and ion-counted images has proven more reliable in determining a proper threshold level than using a source image histogram, the method usually employed in photon counting.⁵ A threshold level is chosen by comparing unprocessed source images with ion-counted images. Several single-shot images are taken prior to accumulation, and a visual comparison is made between the source images and ion-counted images to ensure that the detected ions match the position and number of ions in a single-shot source image. In addition, a visual comparison also determines whether the threshold level is set too high, precluding the detection of ions with intensity levels below the threshold, or too low, producing unwanted detection of low-level noise. The threshold level is adjusted to be between these two limits.

The second step applies an algorithm which locates

maxima in the thresholded data. This procedure gives a final data size for each incoming image between 100 and 300 bytes. The data consist of actual ion addresses. In order to process each image within the 0.1 s allowed by the input data rate, the ion-counting algorithm must be efficient enough to be accommodated by the speed of the DSP. Our solution is based on the property that any 2D function with a local maximum has a positive curvature in both spatial variables at the maximum. Thus, a simple algorithm would be to look for all the pixels with intensities greater than those of their neighboring pixels. However, when digitizing a Gaussian profile into eight bits, plateaus of equal intensity often occur. Thus, additional conditions are required to ensure that a single pixel of the plateau is accepted. The disadvantage of this algorithm is that, for a plateau of $n \times n$ pixels, the selected pixel will be displaced from the center, but by not more than $(\sqrt{n})/2$ pixels. The algorithm we use is to accept all pixels with an intensity $p(x,y)$ which satisfies the following criteria:

$$p(x-1,y) < p(x,y) \geq p(x+1,y), \tag{1}$$

$$p(x,y-1) < p(x,y) \geq p(x,y+1).$$

Once a pixel has passed all of the above inequalities, the corresponding pixel in the final accumulated image is incremented by one; i.e., an ion signal is counted at that location. Thus, each data value at point (x,y) in the final accumulated image represents the total number of ions that have struck that pixel over the entire experiment. To accelerate the accumulation of pixels into the final image buffer, a pixel is summed into the final image the moment it has passed the ion-counting algorithm rather than after all ion candidate pixels have been collected.

As stated above, problems in implementation are most directly related to timing restrictions. The input of source images into the frame grabber, the thresholding algorithm, the location of maxima, and final accumulation into a buffer must all be performed within 0.1 s. For this reason, the latter three procedures have been written in assembly language for the DSP320C40 processor; the procedure for frame grabbing was written in C using the Dipix interface functions. The key idea for implementation of real-time ion counting is to reduce initially large data sets with fast algorithms (thresholding requires only one comparison), and then process the resulting smaller data sets with the more time-consuming algorithms (the determination of local maximum requires four comparisons), thereby minimizing the total time spent on each step of filtering. Further acceleration is accomplished by using parallel processing with two source image buffers. Because the DSP320C40 supports direct memory access (DMA), source images can be acquired from the camera into one buffer while thresholding is being performed in the other.

Figure 1 summarizes the entire ion-counting process.²¹ A minimum of four buffers is required for ion counting. The ion buffer and the collected ion data buffer are optional. Once data is received from a given buffer, it is processed using the appropriate filter, and the results are placed into the next buffer. Data enters from the camera at the top of the

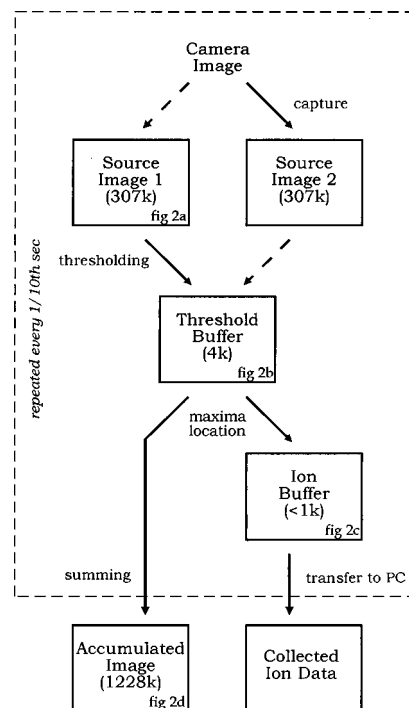


FIG. 1. Schematic diagram for the ion counting method, showing the flow of data. The letters in the boxes representing buffers refer to lettered plates in Fig. 2, which show how the data is processed in each stage of the ion-counting method.

figure and is transferred to source image buffer 2 using low level DMA capture functions from Dipix. At the same time, thresholding is performed on the other source image (buffer 1) using assembly language code, and the results are placed into a threshold buffer. In the next time step, the new source image will be placed in source buffer 1, and thresholding will be performed on source input buffer 2. Data then flows along the dotted paths. After capture and thresholding, the location of maxima is applied to the threshold buffer data, and detected ions are immediately summed into a final accumulated image buffer. Optionally, following the location of maxima the detected ions may also be stored in an ion buffer, where they may be transferred to the PC for a complete, frame-by-frame record of the ion-counting process. The letters in the buffers in Fig. 1 refer to lettered plates in Fig. 2 which show how the data is processed in each stage of the ion-counting method. The fact that data is transferred logically from buffer to buffer through processing filters allows easier and more efficient implementation in assembly language. Note that the threshold and ion buffers are not complete images (with data for every pixel) but maintain only the addresses (offset from the top left of the image) of those pixels holding appropriate signal.

Ultimately, once a pixel is accepted by the ion-counting algorithm, it need only be accumulated into the final product image. However, it is also beneficial to store the addresses of all accepted pixels into a separate ‘ion buffer’ as well. This storage allows later access to the accepted pixels for each frame of the accumulation. A generalization, which would allow access to all of the original data for every frame, will be discussed later.

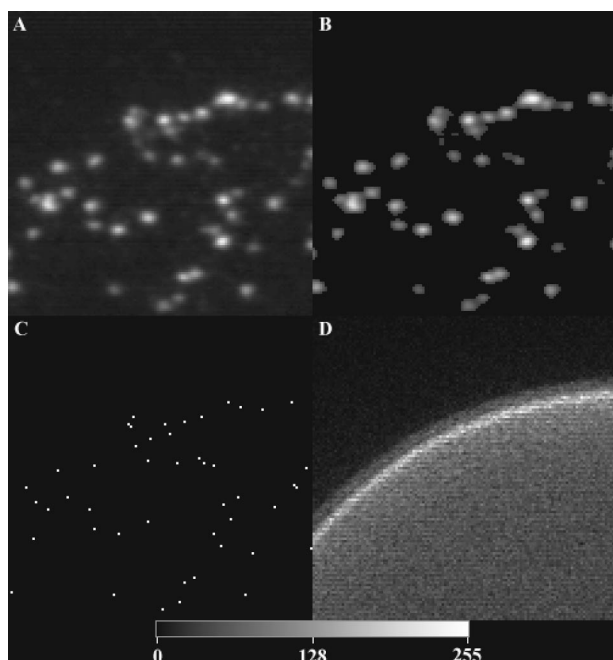


FIG. 2. Typical data shown at various stages of analysis. The lettered figures correspond to the buffers in Fig. 1. (a) Raw data. (b) Thresholded data. (c) Data following local maxima location. (d) Accumulated data. The frame corresponding to panel A has roughly 200 ions. The accumulated signal corresponding to panel D is the sum of 18 000 laser shots.

IV. RESULTS

Figure 3 shows a series of images of $N_2(v''=0, J'' \approx 74)$ ions created by 2 + 1 REMPI following dissociation of N_2O at 203.2 nm. Figures 3(a) and 3(d) show the raw data collected using the traditional accumulation method and the ion-counting method, respectively. Both images were taken using velocity mapping.^{8,9} It is apparent even in the raw data that ion counting provides a significant increase in resolution over the accumulation method, a fact which is even more obvious in the Abel inverse-transformed images shown in Figs. 3(b) and 3(e). The singularity associated with the axis of cylindrical symmetry in the inverse Abel transform causes the vertical line of noise running down the center axes of Figs. 3(b) and 3(e). Figures 3(c) and 3(f) show 8 \times enlargements of Figs. 3(b) and 3(e), respectively. Figure 4 shows translational energy distributions for a selected angle derived from the images of Figs. 3(b) and 3(e). The resolution is higher in the latter case and allows distinction between two peaks in the distribution.

It has been previously observed that absorption by bend (ν_2)-excited N_2O is important in this wavelength region. Even though $N_{v=1}/N_{v=0}$ for the bending mode is only about 6% at room temperature, two closely spaced rings are discernible in the ion-counted images corresponding to the two peaks in the translational energy distribution shown in the full line of Fig. 4. The inner ring results from $N_2(v''=0, J'' \approx 74)$ produced in the dissociation of N_2O in the vibrational

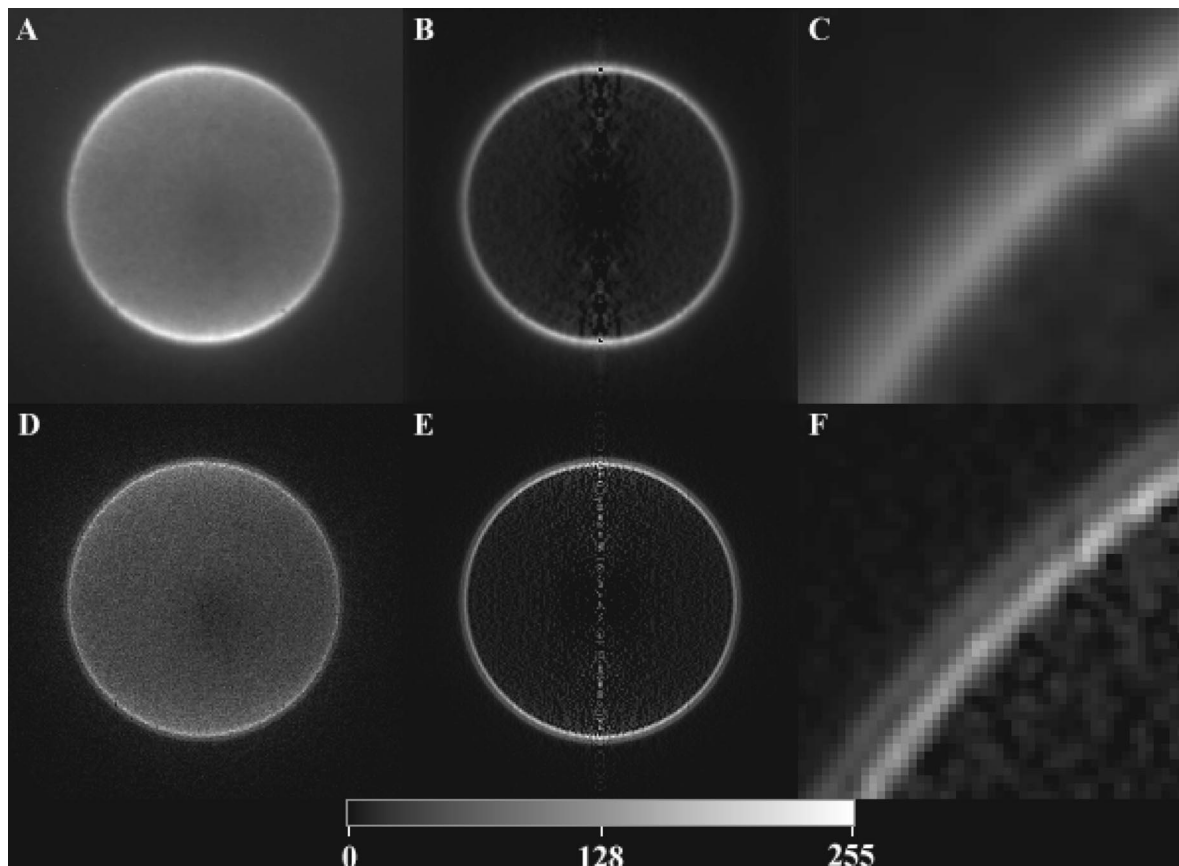


FIG. 3. Panels A and D show images collected using traditional accumulation and using the ion-counting method, respectively, for the $N_2(v''=0, J'' \approx 74)$ product of N_2O photodissociation at 203.2 nm. Panels B and E show the Abel inverse-transformed images of A and D, respectively. Panels 3C and 3F show 8 \times enlargements of B and E, respectively.

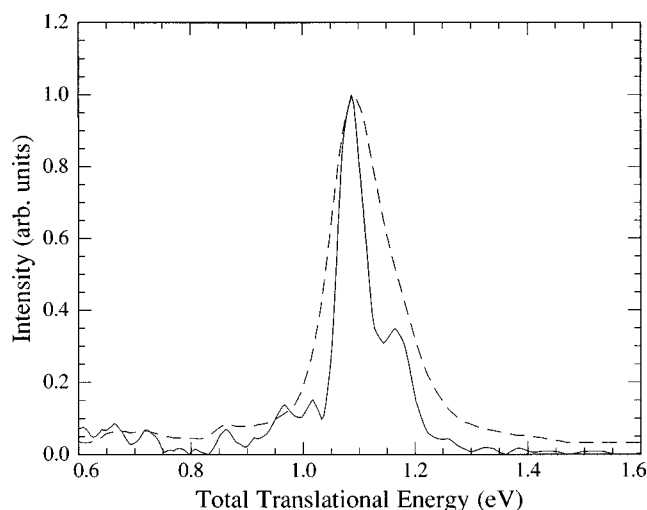


FIG. 4. Translational energy distributions derived for a selected angle from the images in Fig. 3(b) (dashed line) and 3(e) (solid line). It is clear that the energy resolution is higher in the latter case, high enough to resolve two peaks in the distribution.

ground state, and the outer ring from N_2O with one quantum of vibration in the ν_2 bending mode, which has a frequency of 588.78 cm^{-1} . The fact that the intensity in the outer ring is about 26% of the total, much higher than the $\leq 6\%$ expected for a sample at room temperature or lower, supports the thesis that the Franck–Condon factor for the absorption increases with vibrational excitation.

The anisotropy parameters extracted from the data were $\beta = 0.52 \pm 0.05$ and $\beta = 0.50 \pm 0.05$ for accumulation and ion counting methods, respectively, and are in very good agreement with most previously reported values, $\beta \sim 0.5$, by Felder *et al.*,²² Springsteen *et al.*,²³ and Suzuki *et al.*²⁴

V. DISCUSSION

The most important features of ion counting for 2D product imaging include an overall enhancement in spatial resolution and the removal of low-level noise. In addition, ion counting offers the ability to detect ions regardless of variations in peak intensity. The first two of these features result directly from the algorithms used here and have been demonstrated in Fig. 2. However, the third feature is more subtle. Because of inhomogeneities in the spatial response function of both the CCD array and the MCP, and also because of slight differences in the kinetic energy of incoming ions, peak intensities vary from ion to ion even in the same source image. The ion-counting method corrects for this inhomogeneity by assigning a single intensity level to every ion, regardless of its detected peak intensity in the source image. For the single-shot source image in Fig. 2(a), the signal values ranged from 22 to 161 in intensity, giving an overall signal range of 139. The threshold value used for Fig. 2(b) was 35. After ion counting, the lowest ion-counted signal detected was 36, and the highest was 161, giving an ion-counted range of 125. Thus for this single-shot image, ion counting was able to remove any inhomogeneity in detected ion intensity over a dynamic range of $161/36 \approx 4.5$.

Another issue which depends on the number of ions recorded per shot is spatial congestion. In some experiments, the molecule being studied may yield a large number of ions with a relatively small spatial distribution. We call this condition spatial congestion. When it is severe, (where ions are closer than 10 pixels in the source image), the intensity distributions of the neighboring ions are combined, and the location of maxima cannot be performed reliably because the pixel intensities surrounding an ion may not have a regular falloff in intensity. In this case, the ion-counting method may miss an entire cluster of detected ions. So far, the best way we have found to avoid the adverse effects of spatial congestion is to compare a single-shot source image and the ion-counted image to ensure that all ions are being counted and to attenuate the laser light until we meet these conditions.

A more general problem which we observed may also occur in conjunction with spatial congestion. When the total number of ions per frame is relatively high (roughly 500–600 ions, in our case, although not necessarily clustered together), the time required by the DSP to perform ion counting on a single image may be longer than the 0.1 s permitted by the input data rate. In this case, the next incoming image from the camera will be skipped so that processing on the current frame can be completed. Our current solution to this problem is to reduce the signal level.

As addressed in the preceding section, the speed of the DSP limits the number of operations for each incoming image. A traditional method used to locate the centers of the distributions of two-dimensional ion signals is to deconvolute the source image with a two-dimensional operator, for example, a Gaussian function.⁵ This procedure usually gives a good determination of the centers of the distributions but is very time consuming. In 2D photofragment imaging experiments, the high input rate of images precludes its use.

An ideal solution to these problems would be to use a PCI-bus based frame grabber (100 Mbyte/s) to transfer data from the frame grabber to a host computer. For such a bus, the original data from every imaging event may be recorded, and processing can be handled separately, after experimentation. Using this method, the storage of all source images will require 5 GB for a typical experiment (307 Kbytes per frame at 5000 frames), but the decreasing cost of high-speed mass storage devices will make this a feasible alternative for future product imaging experiments. This project is underway in our laboratory. Another alternative is to perform thresholding on the frame grabber and maximum location on the host PC, thereby decreasing the data storage by about 84%.

The real-time ion counting method in 2D product imaging has been demonstrated to extract low-level ion signals and to improve significantly the spatial resolution of the accumulated image. Other methods of increasing the resolution, such as lowering the MCP voltage or not using an image intensifier, restrict application of the imaging method to systems where the signals are larger and where high mass resolution is not needed. The improvements described here will broaden the range of experiments feasible by 2D product imaging by allowing study of cases which have low signal levels.

ACKNOWLEDGMENTS

We are grateful to Nyron Rajab of Dipix Technologies and Richard Sturz of Xybion Electronics for providing technical help in the construction of this image grabbing system. We also thank Dr. Ruth Wilson and Dr. Arthur Suits for stimulating discussions. This work is supported by the National Science Foundation under Grant ATM-9528086, by the Department of Energy under Grant DE-FG02-88ER13934, and by the Research Institute of Innovative Technology for the Earth administered by the New Energy and Industrial Technology Development Organization of Japan.

¹D. W. Chandler and P. L. Houston, *J. Chem. Phys.* **87**, 1445 (1987).

²A. J. R. Heck and D. W. Chandler, *Annu. Rev. Phys. Chem.* **46**, 335 (1995).

³P. L. Houston, *Acc. Chem. Res.* **28**, 453 (1995).

⁴P. L. Houston, *J. Phys. Chem.* **100**, 12 757 (1996).

⁵K. R. Castleman, *Digital Image Processing* (Prentice-Hall, Englewood Cliffs, NJ, 1996).

⁶R. D. Levine and R. B. Bernstein, *Molecular Reaction Dynamics and Chemical Reactivity* (Oxford University Press, New York, 1987).

⁷E. J. Lerner, *Laser Focus World*, 103 (August 1996).

⁸D. H. Parker and A. T. J. B. Eppink, *J. Chem. Phys.* **107**, 2357 (1997).

⁹A. T. J. B. Eppink and D. H. Parker, *Rev. Sci. Instrum.* **68**, 3477 (1997).

¹⁰E. R. Dougherty and P. A. Laplante, *Real-Time Imaging* (IEEE, New Jersey, 1995).

¹¹P. M. Embree, *C Algorithms for Real-Time DSP* (Prentice-Hall, Englewood Cliffs, NJ, 1995).

¹²A. G. Suits, R. L. Miller, L. S. Bontuyan, and P. L. Houston, *J. Chem. Soc., Faraday Trans.* **89**, 1443 (1993).

¹³L. S. Bontuyan, A. G. Suits, P. L. Houston, and B. J. Whitaker, *J. Phys. Chem.* **97**, 6342 (1993).

¹⁴R. L. Miller, A. G. Suits, P. L. Houston, R. Toumi, J. A. Mack, and A. M. Wodtke, *Science* **265**, 1831 (1994).

¹⁵V. P. Hradil, T. Suzuki, S. A. Hewitt, P. L. Houston, and B. J. Whitaker, *J. Chem. Phys.* **99**, 4455 (1993).

¹⁶R. J. Wilson, J. A. Mueller, and P. L. Houston, *J. Phys. Chem. A* **101**, 7593 (1997).

¹⁷D. Proch and T. Trickl, *Rev. Sci. Instrum.* **60**, 713 (1989).

¹⁸The laser calibration was not exact. The rotational level is assigned as $J = 74 \pm 1$.

¹⁹K. R. Lykke and B. D. Kay, *J. Chem. Phys.* **95**, 2252 (1991).

²⁰T. F. Hanisco and A. C. Kummel, *J. Phys. Chem.* **97**, 7242 (1993).

²¹Although the program we use is specific to the frame grabber/camera combination we use, the code may be obtained by writing to the authors.

²²P. Felder, B.-M. Haas, and J. R. Huber, *Chem. Phys. Lett.* **186**, 177 (1991).

²³L. L. Springsteen, S. Satyapal, Y. Matsumi, L. M. Dobeck, and P. L. Houston, *J. Phys. Chem.* **97**, 7239 (1993).

²⁴T. Suzuki, H. Katayanagi, Y. Mo, and K. Tonokura, *Chem. Phys. Lett.* **256**, 90 (1995).